Renewable Energy 116 (2018) 470–478

Contents lists available at ScienceDirect

Renewable Energy

journal homepage: www.elsevier.com/locate/renene

Comparison of wind farm large eddy simulations using actuator disk and actuator line models with wind tunnel experiments

Richard J.A.M. Stevens [a, *], Luis A. Martínez-Tossas [b], Charles Meneveau [b]

[a] Department of Physics, Mesa+ Institute, and J. M. Burgers Centre for Fluid Dynamics, University of Twente, 7500 AE, Enschede, The Netherlands
[b] Department of Mechanical Engineering & Center for Environmental and Applied Fluid Mechanics, Johns Hopkins University, Baltimore, MD 21218, USA

ARTICLE INFO

Article history:
Received 16 September 2016
Received in revised form
19 July 2017
Accepted 26 August 2017
Available online 29 August 2017

Keywords:
Wind farm
Large eddy simulations
Actuator disk model
Actuator line model
Turbine wakes

ABSTRACT

We compare wind farm large eddy simulations with the EPFL wind tunnel measurement by Chamorro and Porté-Agel (Bound-Lay. Meteorol. 136, 515 (2010) and Energies 4, 1916 (2011)). We find that the near turbine wake, up to 3 turbine diameters downstream, of a single turbine is captured better with the actuator line method than using the actuator disk method. Further downstream the results obtained with both models agrees very well with the experimental data, confirming findings from previous studies. For large aligned wind farms we find that the actuator disk model predicts the wake profiles behind turbines on the second and subsequent rows more accurately than the wake profile behind the first turbine row. The reason is that the wake layer profile that is created at hub height in very large wind farms is closer to the assumptions made in the actuator disk model than the logarithmic profile found in the inflow conditions. In addition, we show that, even in relatively coarse resolution simulations, adding the effect of the turbine nacelle and tower leads to a significant improvement in the prediction of the near wake features at 1 and 2 diameters downstream.

1. Introduction

Large eddy simulation (LES) has become a prominent tool for performing high-fidelity numerical simulations of wind farm flows [1,2,3]. When performing wind farm simulations with many turbines, fine grid resolutions are often not affordable. Therefore, coarse resolutions (on the order of 5–10 LES grid points across the rotor) must be used. In this paper we compare the performance of the actuator disk model (ADM) and the actuator line model (ALM) on relatively coarse grids, while we also consider the influence of modeling the nacelle and tower.

The validation of simulation codes against high fidelity experimental data is an important task that has been considered in several recent studies. Here we mention the blind tests workshops by Krogstad et al. [4,5], and Pierella et al. [6] in which the wake evolution behind single or two wind turbines was compared with different simulation and modeling approaches. The WAKEBENCH project [7] provides a comparison between different models for the Sexbierum single wake experiment. Comparisons between wind tunnel experiments, field experiments, and models were a focus of the ENDOW [8] and UPWIND [9] projects, and the well known MEXICO (Model Experiments in Controlled Conditions) experiments [10,11]. For an overview of different wind turbine modeling approaches we refer to the reviews by Sanderse et al. [12] and Sørensen [1]. Comparisons of wind farm LES with field measurement data can, for example, be found in Refs. [2,13,14,15,16,17,18]. Different wind farm modeling approaches are reviewed in Ref. [19].

The blind test comparison by Krogstad et al. [4,5] and Pierella et al. [6], in which different numerical methods are compared with experimental measurements, showed that the lack of a tower and nacelle in simulations results in a high velocity jet in the center of the rotor, which is not observed in measurements. Single turbine simulations, see for example Mittal et al. [20] and Santoni et al. [21], have shown that including the turbine tower and nacelle using an immersed boundary method is important to accurately capture the flow directly behind the wind turbine. Such a detailed approach is not possible for large wind farms, in which the resolution is too coarse to capture tower and nacelle using immersed boundary method. Therefore, attempts have been made to model the tower and nacelle with body forces. Wu and Porté-Agel [22] and Churchfield et al. [23] imposed a steady drag force to mimic the tower and nacelle and showed good agreement with measurement data, while Sarlak et al. [24] used an oscillating force with a

* Corresponding author.
E-mail address: r.j.a.m.stevens@utwente.nl (R.J.A.M. Stevens).

http://dx.doi.org/10.1016/j.renene.2017.08.072

frequency similar to the Strouhal frequency behind the cylinder that agree well with detailed immersed boundary method simulations presented by Santoni et al. [21]. Here we follow a similar approach by modeling the tower and nacelle using body forces and we present a systematic comparison of actuator disk and line model simulations, with and without nacelle, to show that on coarse resolutions this approach indeed gives improved predictions for the velocity profiles directly behind the turbine.

In this study, we validate our LES code for the simulation of a neutral atmospheric turbulent boundary layer flow with the single turbine and aligned wind farm measurements performed by Chamorro and Porté-Agel [25,26]. These measurements have already been used by previous authors to benchmark LES codes, see for example the work by Wu and Porté-Agel [3,22,27], Yang and Sotiropolous [28], Yang et al. [29], and Xie and Archer [30]. In an earlier study we used the Chamorro and Porté-Agel measurements [25,26] to compare ALM simulations with the single turbine case in order to study the effect of spatial filtering on the results in relatively coarse LES [31]. Here we focus on a comparison for the wind farm case [26], while we have now also added results obtained using the ADM for comparison. In section 2 we first introduce the LES approach before providing a detailed discussion on how the concurrent precursor method [32] can be used to reproduce the inflow conditions in the experiment. Subsequently, we introduce the ADM and ALM used to represent the model turbines in our simulation, and address how the turbine nacelle and tower can be included in relatively coarse resolution simulations. In section 3 we discuss the simulation results obtained with the ADM and ALM in comparison to the experimental wind tunnel measurements, and in section 4 we finish with the paper conclusions.

2. Method

We use a LES code that solves the filtered incompressible Navier-Stokes equations using a pseudo-spectral discretization in the horizontal directions and a centered second-order finite differencing scheme in the vertical direction [33,34,35]. In our simulations we use the scale-dependent Lagrangian subgrid model [36]. Coriolis and thermal effects are not specifically included, an approach also used in previous studies such as [22,37,38,39]. A second-order accurate Adams-Bashforth scheme is used for the time integration. Due to the very large Reynolds numbers considered here we parameterize the bottom surface by using a classic wall stress boundary condition [36,40]. This boundary condition relates the wall stress to the velocity at the first grid point using the standard logarithmic similarity law [33]. For the top boundary we use a zero vertical velocity and zero shear stress boundary condition so that the flow studied corresponds effectively to a 'half-channel flow' with an impermeable centerline boundary. The flow is driven by an applied pressure gradient in the x-direction, which in equilibrium determines the wall stress u_*^2 and the velocity scale u_* used to normalize the results of the simulations, together with the domain height H used to normalize length scales. In the remainder of this section we will first address how the inflow conditions obtained in the EPFL experiments can be reproduced in our LES before we discuss the ADM and ALM, and the modeling of the nacelle and tower.

The inflow condition is generated with the concurrent precursor method described in Ref. [32]. In this method the computational domain in the streamwise direction is divided in two sections. In the first section a neutral turbulent atmospheric boundary layer is simulated in a periodic domain using a pressure gradient forcing. Each time step the flow field from this simulation is used to provide the inflow condition for a second section in which the wind farm is placed. In the wind farm section, which is periodic due to the use of spectral methods in the horizontal directions, a long fringe region at the end of the computational section is used to make sure that there is a smooth transition from the flow formed behind the wind farm towards the applied inflow condition. In atmospheric boundary layer simulations a pronounced pattern of high and low velocity speed streaks is formed. We found that these streaks influence the results, especially for this case in which very local profiles are compared. To reduce this effect we average the results over very long times (up to 100 to 200 flow-through times) and very slowly shift the entire flow in the inflow generating domain in the spanwise direction to get well converged (streak independent) results. We note that this method is essentially an automated sequence of "individual" long simulations in which the position of the streaks is shifted with respect to the turbine location to get better statistics (see Munters et al. [41] for a more explicit shifted inflow method).

According to Wu and Porté-Agel [3,22] the roughness height in the wind tunnel experiments [25,42] is 0.03 mm and they report a boundary layer depth of about 0.45 m for the single turbine case and about 0.675 m for the wind farm case. The turbines used in the experiment have a diameter $D = 0.15$ m and the hub height z_h of 0.125 m. To match the inflow conditions from the experiments we set the domain height H in our simulations equal to the reported boundary layer depth δ, i.e. $3D$ for the single turbine case and $4.5D$ for the wind farm case. This defines the ground roughness height $z_{0,\mathrm{lo}}$, which is $z_{0,lo}/H = 6.667 \times 10^{-5}$ for the single turbine case and $z_{0,lo}/H = 4.444 \times 10^{-5}$ for the wind farm case. Fig. 1 shows a sketch of the simulation configuration and Fig. 2 the LES and experimental inflow profiles measured $1D$ in front of the first turbine row. Fig. 2 shows that the LES data capture the experimental profiles quite accurately.

To show how the roughness height $z_{0,lo}$ and boundary layer depth δ can be selected when this information is not directly available we compare the profiles in Fig. 2 with the theoretical estimates for the mean [43].

$$\langle \overline{u} \rangle / u_* = \kappa^{-1} \ln(z/z_{0,lo}) \tag{1}$$

and turbulence intensity [44].

$$\sigma(z) = \frac{\left[\left\langle \overline{(u'^+)^2} \right\rangle\right]^{1/2}}{\langle \overline{u} \rangle} = \frac{[B_1 - A_1 \log(z/\delta)]^{1/2}}{\kappa^{-1} \ln(z_h/z_{0,lo})} \tag{2}$$

observed in high Reynolds number turbulent boundary layer. Here the turbulence intensity is based on the observation of the logarithmic law for the variance

$$\left\langle \overline{(u'^+)^2} \right\rangle = B_1 - A_1 \log(z/\delta), \tag{3}$$

while we use the velocity at hub height for normalization as is done for the experimentally reported measurements [3,22,25,26]. The constants A_1 and B_1, are measured in high Reynolds number turbulent boundary layers experiments, see Marusic et al. [43] for an overview. They concluded that $A_1 \approx 1.25$ is universal, while $B_1 \approx 1.5 - 2.1$ depends on the flow geometry. We previously found that for half channel flow $B_1 \approx 1.6$ gives a good estimation of the velocity fluctuations [40]. Fig. 2 confirms that the theoretical profiles represent the (LES) inflow conditions accurately for $z/\delta \lesssim 0.25$. As δ and $z_{0,lo}$ are the only unknown parameters that determine the mean velocity and turbulence intensity profiles these equations can be used to get a reasonable estimate for these parameters.

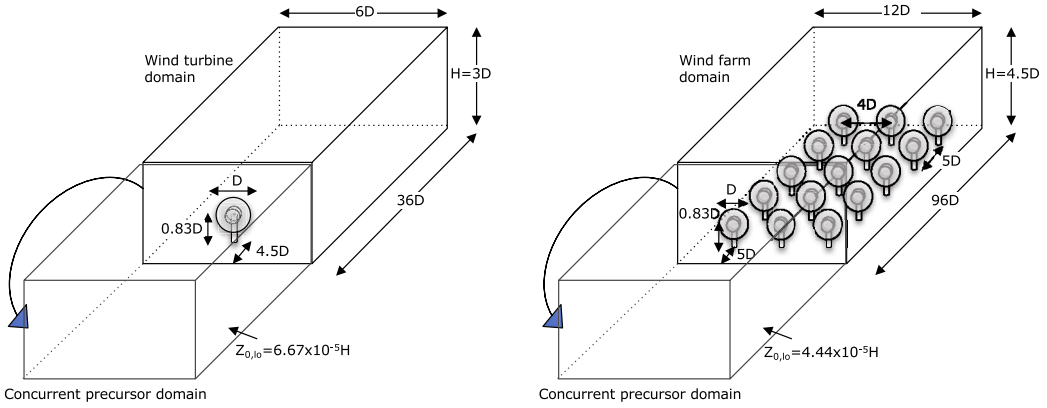

Figure 1. Sketch of the computational domain for the (a) wind turbine and the (b) wind farm simulation. Each time step data from the concurrent precursor domain are sampled and used as inflow condition in the wind turbine/wind farm domain. For clarity the sketch shows only 5 turbine rows for the wind farm domain, while the actual simulations have been performed with 10 turbine rows.

The actuator disk approach, see also Ref. [37,45,46], is based on a drag force (F_t) acting in the streamwise direction according to

$$F_t = -\frac{1}{2}\rho C_T U_\infty^2 \frac{\pi}{4} D^2, \tag{4}$$

where C_T is the thrust coefficient, and U_∞ is an the upstream velocity. This is a good approach when one is modeling a single wind turbine and there are no other interacting bodies in the numerical domain that can make specification of U_∞ ambiguous. When modeling wind farms, it is impossible to define an unperturbed upstream mean velocity since the upstream values are always affected by other upstream wind turbines. It is thus more convenient [37] to use the local velocity at the rotor disk U_d. It can be related to an equivalent upstream unperturbed velocity through the actuator-disk theory $U_\infty = U_d/(1-a)$, where a is the induction factor. Moreover, modeling the thrust forces acting on the fluid due to its interaction with the rotating blades requires the use of an average disk velocity. It is evaluated from LES by averaging over the disk region, and using a first order relaxation method with a typical time of 0.2 s, yielding a velocity denoted by $\langle \overline{u}^T \rangle_d$ [37]. Then, the total thrust force can be written as

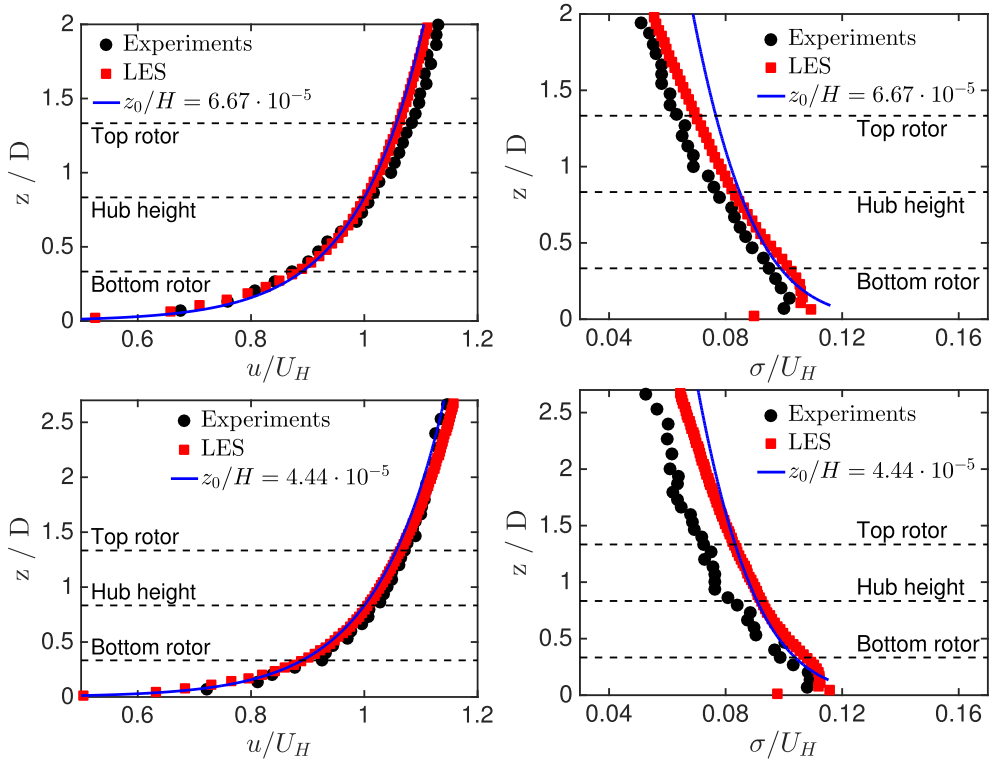

Figure 2. Comparison between the inflow condition obtained in our LES with the measured inflow conditions in the EPFL study by Chamorro and Porté-Agel [25,42]. The top panels indicate the mean and turbulence inflow profiles for the single turbine case and the lower panels for the wind farm case. The lines indicate the theoretical model predictions for the mean (eq. (1)) and the turbulence intensity profiles (eq. (2)), respectively.

Table 1
C_T and C'_T value used for the different rows in the wind farm simulation as obtained from the EPFL measurements by Chamorro and Porté-Agel [3,26].

Case	T_1	T_2	T_3	T_4	T_5
C_T	0.5091	0.5601	0.6406	0.6116	0.5912
C'_T	0.7041	0.8099	1.0015	0.9286	0.8799
Case	T_6	T_7	T_8	T_9	T_{10}
C_T	0.6202	0.6109	0.5898	0.5926	0.5955
C'_T	0.9496	0.9269	0.8768	0.8831	0.8899

$$F_t = -\rho \frac{1}{2} C'_T \langle \overline{u}^T \rangle_d^2 \frac{\pi}{4} D^2, \tag{5}$$

with the subscript d denoting an averaging over the turbine disk region and the superscript T denotes the time averaging and $C'_T = C_T/((1-a)^2)$. Here we use $C_T = 0.5669$ ($C'_T = 0.8248$), which according to Porté-Agel et al. [27] is the thrust coefficient of the turbine in this experiment. For the wind farm case we use the C_T values in Table 1.

The total thrust force is distributed using an indicator function which is determined during code initialization. First the grid-points that fall within each turbine radius are located and subsequently a Gaussian filter $G(x) = [6/(\pi R^2)]^{3/2} \exp(-6 \parallel r \parallel^2 / R^2)$, where r is the distance from the turbine center and $R^2 = h^2(\Delta_x^2 + \Delta_y^2 + \Delta_z^2)$ (where Δ_x, Δ_y, and Δ_z are the mesh-spacings and $h = 1.3$) is used to smooth the indicator function. Reducing the smoothing function further tends to give inaccuracies in the flow solver due to the application of very local forces. The resulting indicator function is normalized with the volume of the turbine disk in order to make sure that the total applied force is independent of the grid resolution. In each grid-point where the indicator function is non-zero a force on the flow that corresponds to the value of the indicator function is applied. This method is similar to the one used in Refs. [37,46].

An ALM has been implemented into the solver by means of body forces [47,48]. The body forces are calculated dynamically using the local velocity at each actuator point. Lift and drag coefficients are obtained from tabulated airfoil data. The body forces are smeared using a Gaussian kernel

$$\eta_\varepsilon = \frac{1}{\varepsilon^3 \pi^{3/2}} e^{-r^2/\varepsilon^2} \tag{6}$$

where r is the distance to the actuator point and ε establishes the width of the kernel. The kernel width is based on the grid resolution with $\varepsilon = 2.5\Delta_x$ [48].

The turbine used in the experiment by Chamorro and Porté-Agel [25,42] is the GWS/EP-6030. In order to determine the lift and drag coefficients for this turbine a low Reynolds number cambered airfoil shape was chosen [49], see the appendix for details. Fig. 3 shows the power and thrust curves calculated using blade element momentum theory (BEM) using the lift and drag coefficient tables shown in the appendix. The turbines are operated at a thrust coefficient of $C_T \approx 0.58$, which coincides with the optimal operational point for the turbine (max C_P). This results in tip speed ratios $\lambda \approx 3.5 - 4.5$.

Since the LES-experiment comparisons will be based on velocity profiles in the center of the wakes, i.e. directly behind the nacelle and the turbine tower, we incorporated the effect of these structures in LES. The turbine nacelle has a diameter of 0.015 m ($0.1D$) and the turbine tower has a diameter of 0.005 m ($0.033D$). The tower and the nacelle are modeled "similar" to the actuator disk using

$$\begin{aligned} F_{nacelle} &= -\rho \frac{1}{2} C'_{nacelle} \langle u \rangle_{nacelle}^2 \frac{\pi}{4} D_{nacelle}^2, \\ F_{tower} &= -\rho \frac{1}{2} C'_{tower} \langle u \rangle_{tower}^2 D_{tower} z_{\mathrm{h}}, \end{aligned} \tag{7}$$

where $C'_{nacelle} = 4$ ($C_{\mathrm{nacelle}} = 1$, i.e. assuming $a = 1/2$) and $C'_{tower} = 0.68$ (i.e. we assume $C_{\mathrm{tower}} = 0.5$ approximately valid for a cylinder, which leads to $a = 0.1464$ using $C_{\mathrm{tower}} = [1 - (1-a)^{0.5}]$). For reference we mention that Wu and Porté-Agel [22] use $C_{\mathrm{nacelle}} = 0.8$ and $C_{\mathrm{tower}} = 1.2$, and Sarlak et al. [24] set $C_{\mathrm{tower}} = 1.2$ without modeling a specific nacelle. We note that this modeling only captures the "global" effects of the nacelle and tower but considering the very coarse resolution (especially the turbine tower is much smaller than the grid resolution) the nacelle and tower cannot be represented using, for example an immersed boundary method [20,21] in the present simulation setup. Here the goal is to test the effect of the nacelle and tower on grids that are typically used in wind farm simulations. Just as for the ADM we use a blending coefficient $h = 1.3$ for the nacelle and tower forces. We note that especially the profiles at 1 diameter downstream can be sensitive to small details in the modeling such as the used blending function.

3. Results

For the single turbine case we use a computational domain size of $36D \times 6D \times 3D$ in the streamwise, spanwise, and vertical directions. respectively, that is discretized on a mesh with $384 \times 64 \times 72$

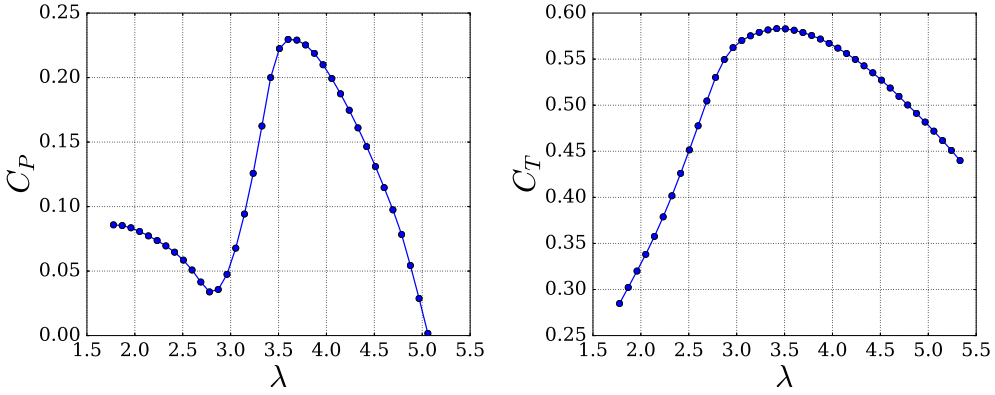

Figure 3. Power (left) and thrust (right) coefficients computed using blade element momentum theory with lift and drag coefficients from a cambered plate at low Reynolds number [49], see also the appendix.

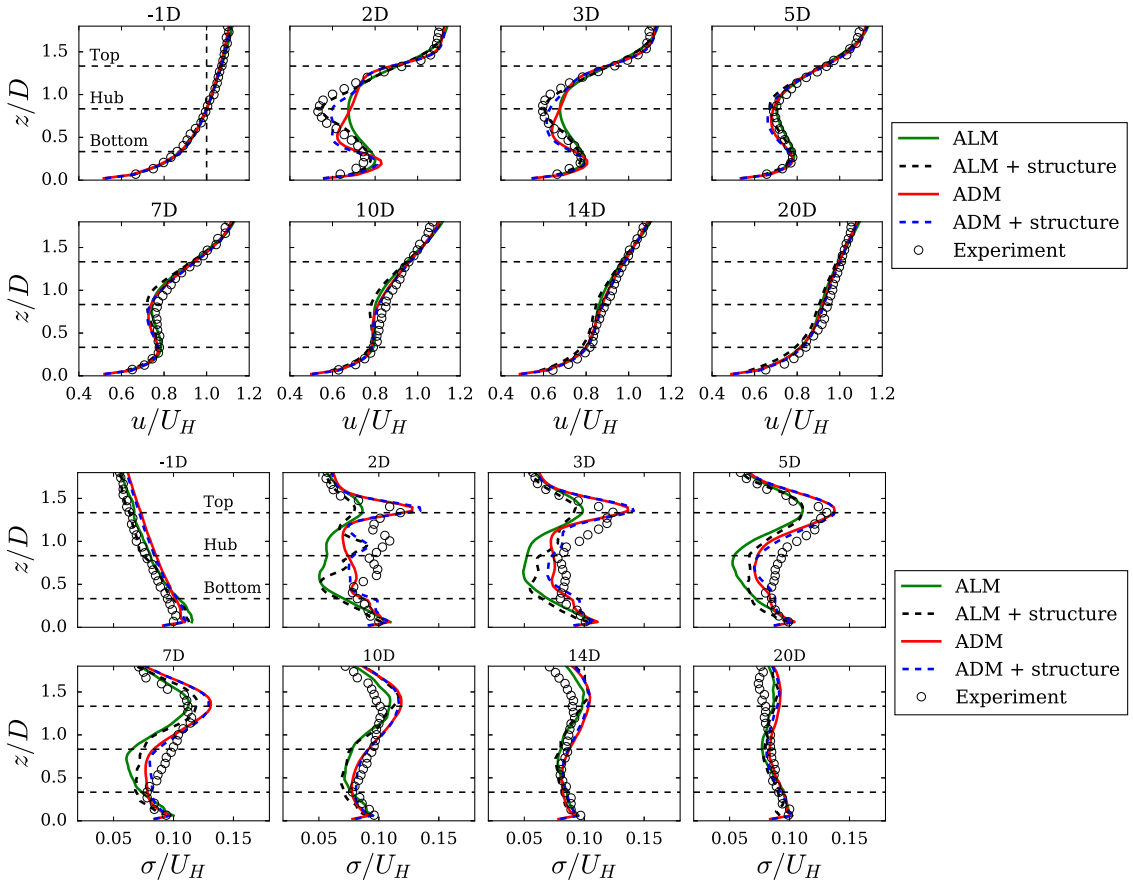

Figure 4. Comparison between the EPFL measurements by Chamorro and Porté-Agel [25] and our simulation results using the ADM and ALM. The top panels show the average streamwise velocity at different downstream distances behind the turbine and the lower panels the corresponding streamwise turbulence intensity profiles. The dashed and solid lines indicate the results with and without the turbine nacelle and tower, i.e. the structure, as indicated in the legend.

computational nodes. Therefore the average grid scale $\Delta = (\Delta_x\Delta_y\Delta_z)^{1/3}$ compared to the turbine diameter D is $\Delta/D = 0.0715$, and the used ground roughness height $z_{0,\mathrm{lo}}/\delta = 6.667 \times 10^{-5}$ where $\delta = 3D$ is the domain height. The center of the turbine is placed at $4.5D \times 3D \times 0.8333D$, while the large streamwise and spanwise domain lengths ensure that the results are domain independent.

Fig. 4 shows a comparison of the mean streamwise velocity profiles obtained from the simulations with the wind tunnel data [22,25]. The profiles are obtained in the centerline of the turbine, where also the tower and the nacelle are located. In agreement with literature results [3,19,22,27,28,29,45] we find that starting at 3 turbine diameters downstream the velocity profile obtained using the ADM and ALM match the results obtained from the experiments closely. Fig. 4 reveals that the near wake velocity profiles obtained in the simulations match the experimentally obtained profiles significantly better when the turbine tower and nacelle are incorporated, i.e. due to the addition of the nacelle and tower the very low velocity in the near wake is now captured. This indicates that it is important to incorporate tower and nacelle in the modeling when considering the local profiles in the center of the wake directly behind the turbine structure. About 5 turbine diameters behind the turbines the effect of the nacelle and tower become negligible even in these local profiles. Here we also note that in this experiment the nacelle and tower are quite large compared to the turbine diameter, and for field scale turbines the effects on these local profiles will therefore be smaller.

When we look at the turbulence intensity profiles we see that the addition of the nacelle and tower improves the prediction of the turbulence peak in the near wake at hub height. The additional turbulence intensity generated by the turbine and nacelle wakes is captured when the tower and nacelle are included as then tower and nacelle wakes are captured as far as the coarse grid allows. We also see that the ALM tends to predict a lower turbulence intensity in the wake than the ADM. We varied the kernel width ε in the ALM and did not find any significant change, so we do not know the exact reason for this difference. We note that the difference could be caused by the relatively low resolution of the presented

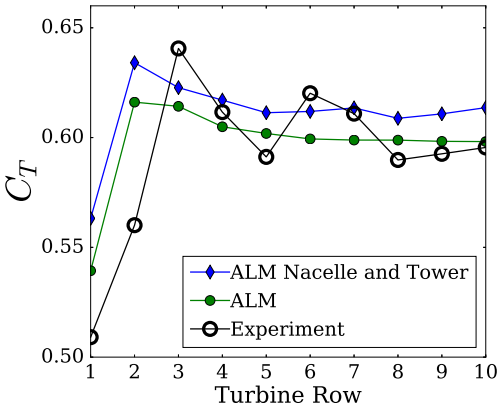

Figure 5. Thrust coefficient for each row using the ALM with and without nacelle and tower compared to the experimental results by Chamorro and Porté-Agel [42].

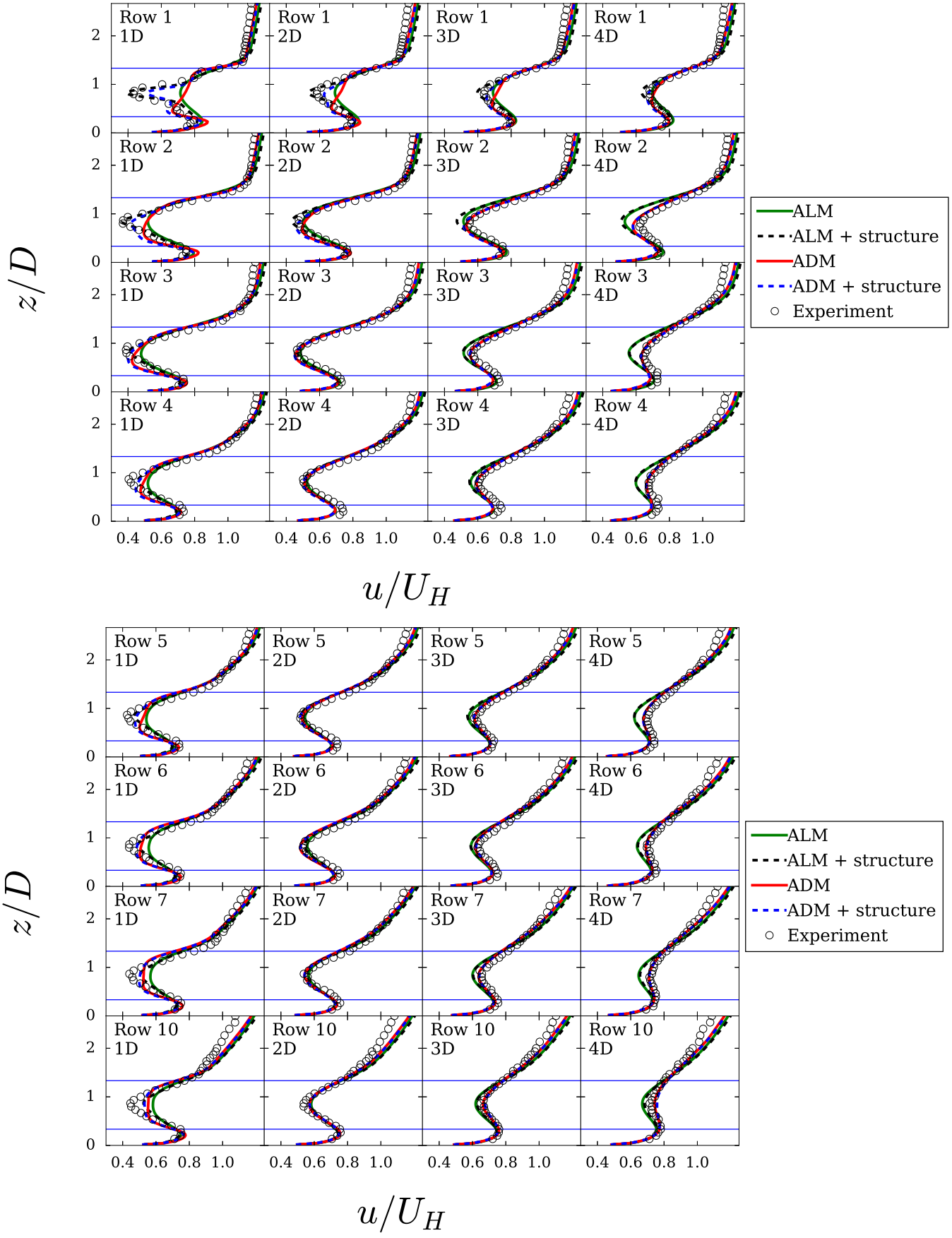

Figure 6. Comparison between the mean streamwise velocity profiles obtained from our LES with ADM and ALM with the EPFL measurements by Chamorro and Porté-Agel [42]. The panels from top to bottom and left to right indicate the mean streamwise velocity profiles as function of height at several distances behind the turbines for the different turbine rows. The dashed and solid lines indicate the results with and without the turbine nacelle and tower, i.e. the structure, as indicated in the legend. The horizontal lines indicate the bottom and top of the turbine rotor.

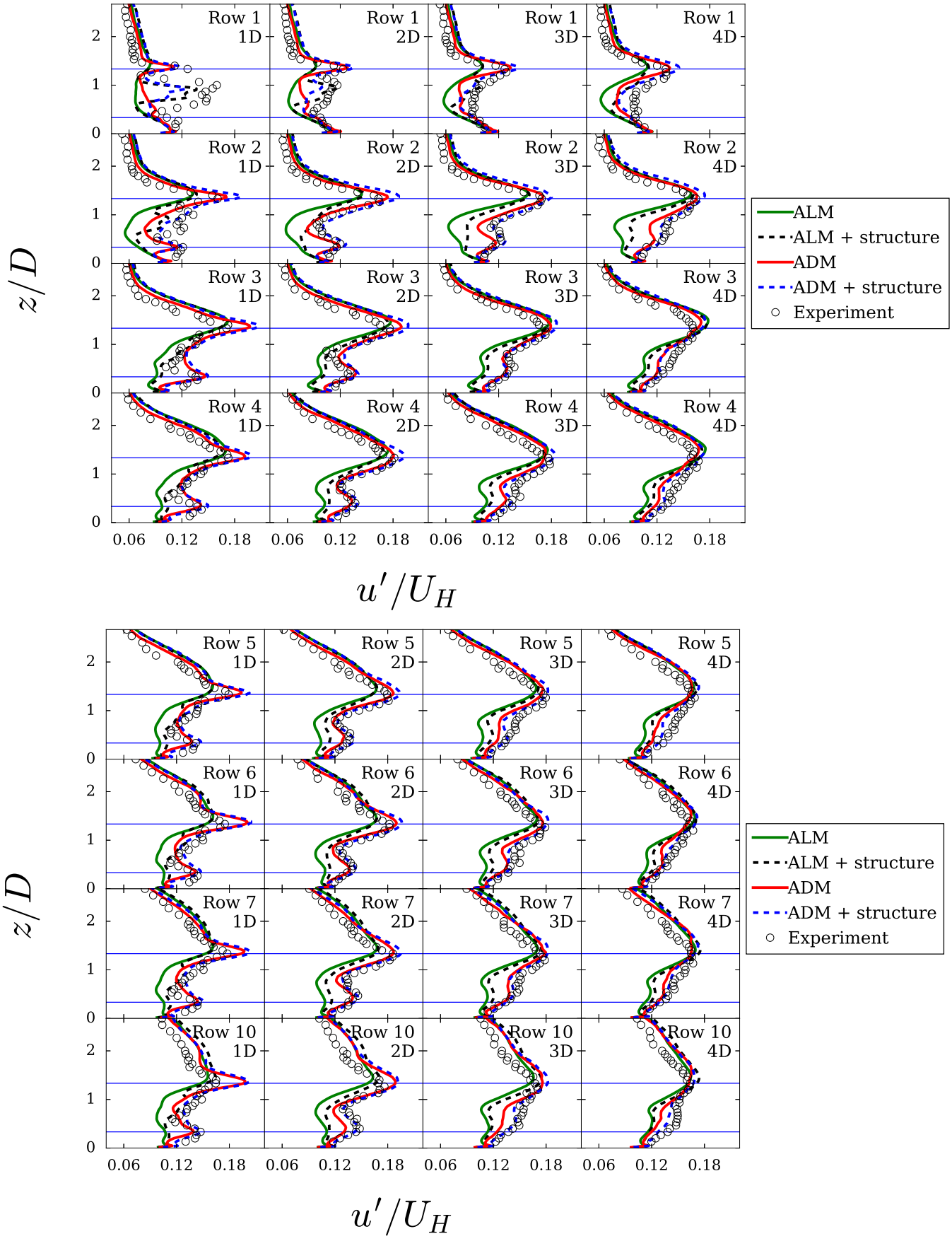

Figure 7. Comparison between the streamwise turbulence intensity profiles obtained from our LES with ADM and ALM with the EPFL measurements by Chamorro and Porté-Agel [42]. The panels from top to bottom and left to right indicate the mean streamwise velocity profiles as function of height at several distances behind the turbines for the different turbine rows. The dashed and solid lines indicate the results with and without the turbine nacelle and tower, i.e. the structure, as indicated in the legend. The horizontal lines indicate the bottom and top of the turbine rotor.

simulations, see for example Ref. [31] where we discuss the effect of numerical resolution on ALM results.

For the wind farm case we use a computational domain of $96D \times 12D \times 4.5D$ in the streamwise, spanwise, and vertical direction, respectively. The used grid resolution for this case is $1024 \times 128 \times 144$, which means $\Delta = (\Delta_x\Delta_y\Delta_z)^{1/3}/D = 0.0650$, while we use a roughness height $z_{0,\mathrm{lo}}/\delta = 4.444 \times 10^{-5}$. The wind farm has 10 rows in the streamwise direction and 3 columns in the spanwise direction (using periodic boundary conditions) with spacing of $5D$ and $4D$ respectively, which start at $5D$ from the domain entrance. When the ALM is used the rotational speed for the turbines needs to be specified in the model. In this case, a special torque controller [31] was chosen such that the tip speed ratio was fixed for each row. The tip speed ratio was chosen according to the computations generated using BEM theory, see Fig. 3, to provide the correct thrust coefficient. The ALM cannot replicate the results form BEM exactly [31], thus the thrust coefficients obtained in the simulation are slightly different than what is expected as seen in Fig. 5. The ADM does not have this issue since it can, by definition, match the thrust coefficient exactly. Although it must be noted that the thrust coefficient has to be specified in the ADM a priori while the ALM does not require this input.

The mean velocity profiles for the wind farm case are shown in Fig. 6. Overall we find a very good agreement between both the ADM and ALM and the wind tunnel measurements [26]. In agreement with the single turbine case we find that the profiles 1 diameter downstream are represented more accurately when the effect of the nacelle and tower is incorporated. We observe that the prediction of the near wake profile, i.e. less than $3D$ downstream of a turbine, for turbines further downstream obtained using the ADM simulations significantly improve. The reason is that the wake layer profile that is created at hub height in very large wind farms is closer to the assumptions made in the ADM, i.e. the averaging of the force over the disk area, than the logarithmic profile found in the inflow conditions. As the ALM does not make this assumption the near wake profiles behind each turbine row are predicted with similar accuracy. In addition, we notice that the effect of the nacelle and tower on the wake profiles is less pronounced for further downstream rows. This is an effect of the slower wind velocity in front of downstream rows (compared to the inflow velocity at the first turbine row). Therefore the additional drag experienced by the nacelle and tower is less for turbines deeper in the wind farm array. For further downstream rows we see that the ALM predicts slightly larger wake deficits, which is due to the slightly higher C_T coefficient that is predicted by the ALM, see Fig. 5. In Fig. 7 we see that for the ADM the most significant differences in the turbulence intensity profiles are observed directly behind the first turbine row, where the addition of the nacelle and tower leads to improved results, while in profiles further downstream the agreement between LES and experiments is very good. In agreement with the single turbine case we find that the ALM model tends to predict somewhat lower turbulence intensities in the wake region just behind the turbine. This difference is washed out after about 4 turbine diameters, so before the next turbine row.

We note that the emphasis of this paper has been on the wakes and the flow rather than power, which requires more work and in this case also no power data is available from the experiments [25,26]. In addition, we know that coarse-LES ALM is bad in terms of predictions of power [48], while for ADM it depends on the accuracy of tabulated C_t and C_p values. In the wind farm simulation using the ADM adding the tower and nacelle leads to a difference of at most 2% in the mean velocity measured at the turbine location and for most turbines the difference is significantly lower. For the ALM the observed difference is about 15%.

4. Conclusions

A detailed comparison of large eddy simulations (LES) using an actuator disk model (ADM) and an actuator line model (ALM), with and without tower and nacelle, with wind tunnel experiments performed at EPFL by Chamorro and Porté-Agel [25,42] reveals generally good agreement. We find that it is particularly important to accurately represent the inflow conditions in the experiments and to apply sufficient averaging in order to eliminate the effect of the high and low velocity speed streaks that are formed in the boundary layer. A comparison between the different simulations reveals that incorporating of the nacelle and tower is very important to reproduce the larger wake deficits and higher turbulence intensities that are measured in the center of the wake just behind the nacelle and tower. In contrast to some earlier literature results [3,12,22,28,29] we show that a standard ADM with additional nacelle and tower already captures the mean and turbulence intensity profiles at 1 and 2 diameters downstream quite accurately, even on very coarse grids. This observation that modeling the nacelle and tower with body forces is beneficial is in agreement with earlier work by Wu and Porté-Agel [22], Churchfield et al. [23], and Sarlak et al. [24] as discussed above. In the wind farm case we see that, due to the formation of the wake layer at hub height, the predictions of the ADM match the experimental observations even closer further downstream in the wind farm. It thus seems that the ADM can be a suitable method to represent turbines in LES of very large wind farms, provided that one is interested in the main flow structures. As the ADM does not represent the actual movement of the blades, the detailed blade properties, etc. it cannot capture flow details such as tip vortices that are captured well using high resolution ALM simulation [1,12]. As we focused on the performance of the ADM and ALM model in relatively coarse resolution simulations we did not obtain this high resolution regime in which the ALM holds significant advantages over the ADM although the ALM can in principle provide more detailed information about radial distributions of blade loadings etc.

Acknowledgements

We thank Ting Wu and Fernando Porté-Agel for providing the experimental data of the wind farm case for comparison and Stefano Leonardi for discussions. RS is funded in part by the research program 'Fellowships for Young Energy Scientists' (YES!) of the Foundation for Fundamental Research on Matter (FOM) supported by the Netherlands Organization for Scientific Research (NWO) and by the Shell-NWO/FOM-initiative Computational sciences for energy research of Shell and Chemical Sciences, Earth and Live Sciences, Physical Sciences, FOM and STW. Further partial support has been provided by the US National Science Foundation from grant OISE-1243482 (WINDINSPIRE) and 1230788. This work used the Extreme Science and Engineering Discovery Environment (XSEDE), which is supported by the National Science Foundation grant number OCI-1053575 and using the national e-infrastructure of SURFsara, a subsidiary of SURF cooperation, the collaborative ICT organization for Dutch education and research. Computational resources were also provided by the Maryland Advanced Research Computing Center (MARCC).

Appendix

Table 2 shows the lift and drag coefficients of Airfoil 8 from Sunada et al. [49]. To the best of our knowledge, Airfoil 8 from Sunada et al. [49] is the most similar blade to the blades used in the model wind turbine in the Chamorro and Porté-Agel experiments [25,27] for which aerodynamic data could be found in the

literature. These values have been used in the BEM calculations that result in the power and thrust curves shown in Fig. 3.

Table 2
Lift and drag coefficients used for the airfoil profiles of a GWS/EP-6030 [49].

α	c_l	c_d	α	c_l	c_d
−20.0	−0.572	0.402	2.0	0.354	0.073
−18.0	−0.555	0.321	4.0	0.591	0.083
−16.0	−0.536	0.251	6.0	0.804	0.136
−14.0	−0.512	0.228	8.0	0.957	0.307
−12.0	−0.488	0.203	10.0	1.032	0.400
−10.0	−0.464	0.176	12.0	1.016	0.400
−8.0	−0.424	0.153	14.0	0.995	0.400
−6.0	−0.370	0.135	16.0	0.971	0.400
−4.0	−0.240	0.114	18.0	0.976	0.400
−2.0	−0.083	0.092	20.0	0.987	0.400
0.0	0.132	0.081			

References

[1] J.N. Sørensen, Aerodynamic aspects of wind energy conversion, Annu. Rev. Fluid Mech. 43 (2011) 427.
[2] M.J. Churchfield, S. Lee, P.J. Moriarty, L.A. Martínez, S. Leonardi, G. Vijayakumar, J.G. Brasseur, A large-eddy simulation of wind-plant aerodynamics, in: 50th AIAA Aerospace Sciences Meeting Including the New Horizons Forum and Aerospace Exposition, 09–12 January 2012, AIAA, Nashville, Tennessee, 2012, 2012-0537.
[3] Y.T. Wu, F. Porté-Agel, Simulation of turbulent flow inside and above wind farms: model validation and layout effects, Bound-Lay. Meteorol. 146 (2013) 181.
[4] P.Å. Krogstad, P.E. Eriksen, "Blind test" calculations of the performance and wake development for a model wind turbine, Renew. Energy 50 (2013) 325.
[5] P.Å. Krogstad, L. Sætran, M.S. Adaramola, "Blind Test 3" calculations of the performance and wake development behind two in-line and offset model wind turbines, J. Fluids Struct. 52 (2015) 65.
[6] F. Pierella, P.Å. Krogstad, L. Sætran, Blind Test 2 calculations for two in-line model wind turbines where the downstream turbine operates at various rotational speeds, Renew. Energy 70 (2014) 62.
[7] P.J. Moriarty, J.S. Rodrigo, P. Gancarski, M. Chuchfield, J.W. Naughton, K.S. Hansen, E. Machefaux, E. Maguire, F. Castellani, L. Terzi, S.P. Breton, Y. Ueda, IEA-Task 31 WAKEBENCH: towards a protocol for wind farm flow model evaluation. Part 2: wind farm wake models, J. Phys. Conf. Ser. 524 (2014), 012185.
[8] R. Barthelmie, G. Larsen, S. Pryor, H. Jørgensen, H. Bergström, W. Schlez, K. Rados, B. Lange, P. Vølund, S. Neckelmann, S. Mogensen, G. Schepers, T. Hegberg, L. Folkerts, M. Magnusson, ENDOW (EfficieNt Development of Offshore Wind farms): modelling wake and boundary layer interactions, Wind Energy 7 (2004) 225.
[9] R.J. Barthelmie, S.T. Frandsen, O. Rathmann, K. Hansen, E.S. Politis, J. Prospathopoulos, J.G. Schepers, K. Rados, D. Cabezón, W. Schlez, A. Neubert, M. Heath, Flow and Wakes in Large Wind Farms: Final Report for UpWind WP8, 2011. Report number Risø-R-1765(EN).
[10] J.G. Schepers, K. Boorsma, T. Cho, S. Gomez-Iradi, P. Schaffarczyk, A. Jeromin, W.Z. Shen, T. Lutz, K. Meister, B. Stoevesandt, S. Schreck, D. Micallef, R. Pereira, T. Sant, H.A. Madsen, N. Sørensen, Final Report of IEA Task 29, Mexnext (Phase 1): Analysis of MEXICO Wind Tunnel Measurements, 2007. ECN report ECN-E12–E1004.
[11] K. Boorsma, J.G. Schepers, New MEXICO Experiment Preliminary Overview with Initial Validation, 2014. ECN report ECN-E-14-048, 1.
[12] B. Sanderse, S.P. van der Pijl, B. Koren, Review of computational fluid dynamics for wind turbine wake aerodynamics, Wind Energy 14 (2011) 799.
[13] S. S. M. Ivanell, Ph.D. Thesis, Dept. of Mechanics, Gotland Univ., Stockholm, Sweden, 2009.
[14] F. Porté-Agel, Y.T. Wu, C.H. Chen, A numerical study of the effects of wind direction on turbine wakes and power losses in a large wind farm, Energies 6 (2013) 5297.
[15] Y.T. Wu, F. Porté-Agel, Modeling turbine wakes and power losses within a wind farm using LES: an application to the Horns Rev offshore wind farm, Renew. Energy 75 (2015) 945.
[16] A. Creech, W.G. Früh, A.E. Maguire, Simulations of an offshore wind farm using large-eddy simulation and a torque-controlled actuator disc model, Surv. Geophys 36 (2015) 427.
[17] K. Nilsson, S. Ivanell, K.S. Hansen, R. Mikkelsen, J.N. Sørensen, S.P. Breton, D. Henningson, Large-eddy simulations of the Lillgrund wind farm, Wind Energy 18 (2015) 449.
[18] O. Eriksson, J. Lindvall, S.P. Breton, S. Ivanell, Wake downstream of the Lillgrund wind farm - a comparison between LES using the actuator disc method and a wind farm parametrization in WRF, J. Phys. Conf. Ser. 625 (2015), 012028.
[19] R.J.A.M. Stevens, C. Meneveau, Flow structure and turbulence in wind farms, Annu. Rev. Fluid Mech. 49 (2017) 311.
[20] A. Mittal, K. Sreenivas, L.K. Taylor, L. Hereth, C.B. Hilbert, Blade-resolved simulations of a model wind turbine: effect of temporal convergence, Wind Energy 19 (2016) 1761.
[21] C. Santoni, K. Carrasquillo, I. Arenas-Navarro, S. Leonardi, Effect of tower and nacelle on the flow past a wind turbine, Wind Energy (2017) 1–13, http://dx.doi.org/10.1002/we.2130.
[22] Y.T. Wu, F. Porté-Agel, Large-eddy simulation of wind-turbine wakes: evaluation of turbine parametrisations, Bound-Lay. Meteorol. 138 (2011) 345.
[23] M.J. Churchfield, Z. Wang, S. Schmitz, Modeling wind turbine tower and nacelle effects within an actuator line model, in: 33rd Wind Energy Symposium, AIAA SciTech AIAA 2015, 2015.
[24] H. Sarlak, C. Meneveau, J.N. Sørensen, Role of subgrid-scale modeling in large eddy simulation of wind turbine wake interactions, Renew. Energy 77 (2015) 386.
[25] L.P. Chamorro, F. Porté-Agel, Effects of thermal stability and incoming boundary-layer flow characteristics on wind-turbine wakes: a wind-tunnel study, Bound-Lay. Meteorol. 136 (2010) 515.
[26] M. Chamecki, C. Meneveau, Particle boundary layer above and downstream of an area source: scaling, simulations, and pollen transport, J. Fluid Mech. 683 (2011) 1.
[27] F. Porté-Agel, Y.T. Wu, H. Lu, R.J. Conzemius, Large-eddy simulation of atmospheric boundary layer flow through wind turbines and wind farms, J. Wind Eng. Ind. Aerodyn 99 (2011) 154.
[28] X. Yang, F. Sotiropoulos, On the predictive capabilities of LES-actuator disk model in simulating turbulence past wind turbines and farms, in: 2013 American Control Conference (ACC), Institute of Electrical and Electronics Engineers (IEEE), Washington, DC, USA, 2013, p. 2878. June 17-19 2013.
[29] D. Yang, C. Meneveau, L. Shen, Large-eddy simulation of offshore wind farm, Phys. Fluids 26 (2014), 025101.
[30] S. Xie, C. Archer, Self-similarity and turbulence characteristics of wind turbine wakes via large-eddy simulation, Wind Energy 18 (2015) 1815.
[31] L.A. Martínez-Tossas, R.J.A.M. Stevens, C. Meneveau, Wind farm large-eddy simulations on very coarse grid resolutions using an actuator line model, in: 34th Wind Energy Symposium, AIAA SciTech, AIAA, 2016, 2016-1261, 1.
[32] R.J.A.M. Stevens, J. Graham, C. Meneveau, A concurrent precursor inflow method for Large eddy simulations and applications to finite length wind farms, Renew. Energy 68 (2014) 46.
[33] C.H. Moeng, A large-eddy simulation model for the study of planetary boundary-layer turbulence, J. Atmos. Sci. 41 (1984) 2052.
[34] J.D. Albertson, M.B. Parlange, Surface length-scales and shear stress: implications for land-atmosphere interaction over complex terrain, Water Resour. Res. 35 (1999) 2121.
[35] F. Porté-Agel, C. Meneveau, M.B. Parlange, A scale-dependent dynamic model for large-eddy simulation: application to a neutral atmospheric boundary layer, J. Fluid Mech. 415 (2000) 261.
[36] E. Bou-Zeid, C. Meneveau, M.B. Parlange, A scale-dependent Lagrangian dynamic model for large eddy simulation of complex turbulent flows, Phys. Fluids 17 (2005), 025105.
[37] M. Calaf, C. Meneveau, J. Meyers, Large eddy simulations of fully developed wind-turbine array boundary layers, Phys. Fluids 22 (2010), 015110.
[38] H. Lu, F. Porté-Agel, Large-eddy simulation of a very large wind farm in a stable atmospheric boundary layer, Phys. Fluids 23 (2011), 065101.
[39] M. Calaf, C. Higgins, M.B. Parlange, Large wind farms and the scalar flux over an heterogeneously rough land surface, Bound-Lay. Meteorol. 153 (2014) 471.
[40] R.J.A.M. Stevens, M. Wilczek, C. Meneveau, Large eddy simulation study of the logarithmic law for high-order moments in turbulent boundary layers, J. Fluid Mech. 757 (2014) 888.
[41] W. Munters, C. Meneveau, J. Meyers, Shifted periodic boundary conditions for simulations of wall-bounded turbulent flows, Phys. Fluids 28 (2016), 025112.
[42] L.P. Chamorro, F. Porté-Agel, Turbulent flow inside and above a wind farm: a wind-tunnel study, Energies 4 (2011) 1916.
[43] I. Marusic, J.P. Monty, M. Hultmark, A.J. Smits, On the logarithmic region in wall turbulence, J. Fluid Mech. 716 (2013) R3.
[44] R.J.A.M. Stevens, D.F. Gayme, C. Meneveau, Using the coupled wake boundary layer model to evaluate the effect of turbulence intensity on wind farm performance, J. Phys. Conf. Ser. 625 (2015), 012004.
[45] A. Jiménez, A. Crespo, E. Migoya, J. Garcia, Advances in large-eddy simulation of a wind turbine wake, J. Phys. Conf. Ser. 75 (2007), 012041.
[46] M. Calaf, M.B. Parlange, C. Meneveau, Large eddy simulation study of scalar transport in fully developed wind-turbine array boundary layers, Phys. Fluids 23 (2011), 126603.
[47] J.N. Sørensen, W.Z. Shen, Numerical modeling of wind turbine wakes, J. Fluids Eng. 124 (2002) 393.
[48] L.A. Martínez-Tossas, M.J. Churchfield, S. Leonardi, Large eddy simulations of the flow past wind turbines: actuator line and disk modeling, Wind Energy 18 (2015) 1047.
[49] S. Sunada, A. Sakaguchi, K. Kawachi, Airfoil section characteristics at a low Reynolds number, J. Fluids Eng. 119 (1997) 129.